RESEARCH ARTICLE

Insights into Hydrocarbon Formation by Nitrogenase Cofactor Homologs

Chi Chung Lee,[a] Yilin Hu,[a] Markus W. Ribbe[a,b]

Department of Molecular Biology and Biochemistry, University of California, Irvine, Irvine, California, USA[a]; Department of Chemistry, University of California, Irvine, Irvine, California, USA[b]

ABSTRACT **The L-cluster is an all-iron homolog of nitrogenase cofactors. Driven by europium(II) diethylenetriaminepentaacetate [Eu(II)-DTPA], the isolated L-cluster is capable of ATP-independent reduction of CO and CN^- to C_1 to C_4 and C_1 to C_6 hydrocarbons, respectively. Compared to its cofactor homologs, the L-cluster generates considerably more CH_4 from the reduction of CO and CN^-, which could be explained by the presence of a "free" Fe atom that is "unmasked" by homocitrate as an additional site for methanation. Moreover, the elevated CH_4 formation is accompanied by a decrease in the amount of longer hydrocarbons and/or the lengths of the hydrocarbon products, illustrating a competition between CH_4 formation/release and C−C coupling/chain extension. These observations suggest the possibility of designing simpler synthetic clusters for hydrocarbon formation while establishing the L-cluster as a platform for mechanistic investigations of CO and CN^- reduction without complications originating from the heterometal and homocitrate components.**

IMPORTANCE **Nitrogenase is a metalloenzyme that is highly complex in structure and uniquely versatile in function. It catalyzes two reactions that parallel two important industrial processes: the reduction of nitrogen to ammonia, which parallels the Haber-Bosch process in ammonia production, and the reduction of carbon monoxide to hydrocarbons, which parallels the Fischer-Tropsch process in fuel production. Thus, the significance of nitrogenase can be appreciated from the perspective of the useful products it generates: (i) ammonia, the "fixed" nitrogen that is essential for the existence of the entire human population; and (ii) hydrocarbons, the "recycled" carbon fuel that could be used to directly address the worldwide energy shortage. This article provides initial insights into the catalytic characteristics of various nitrogenase cofactors in hydrocarbon formation. The reported assay system provides a useful tool for mechanistic investigations of this reaction while suggesting the possibility of designing bioinspired catalysts based on nitrogenase cofactors.**

Received 23 February 2015 **Accepted** 25 March 2015 **Published** 14 April 2015

Citation Lee CC, Hu Y, Ribbe MW. 2015. Insights into hydrocarbon formation by nitrogenase cofactor homologs. mBio 6(2):e00307-15. doi:10.1128/mBio.00307-15.

Editor Douglas G. Capone, University of Southern California

Address correspondence to Markus W. Ribbe, mribbe@uci.edu.

This article is a direct contribution from a Fellow of the American Academy of Microbiology.

Nitrogenase catalyzes the reduction of various substrates, such as nitrogen (N_2), carbon monoxide (CO), and cyanide (CN^-), at its cofactor site (1–4). The molybdenum (Mo)- and vanadium (V)-nitrogenases are two homologous members of this enzyme family, and they contain homologous cofactors, namely, the molybdenum-iron cofactor (FeMoco or M-cluster) and the vanadium-iron cofactor (FeVco or V-cluster), at their respective active sites (2, 5, 6). The M-cluster (Fig. 1) is a $[MoFe_7S_9C]$ cluster that consists of $[Fe_4S_3]$ and $[MoFe_3S_3]$ subclusters bridged by three μ_2-sulfides and a μ_6-carbide, and the Mo end of this cofactor is further associated with a homocitrate entity (7–10). Substituted by V in place of Mo, the V-cluster (Fig. 1) is nearly indistinguishable from the M-cluster in structure, although the presence of an interstitial carbide is yet to be demonstrated (6). Other than the two cofactors, a so-called L-cluster has been identified both as a precursor and a structural homolog to the M-cluster. This homocitrate-free cluster has a composition of $[Fe_8S_9C]$ (Fig. 1), and it closely resembles the metal-sulfur core of a mature M-cluster (11–15).

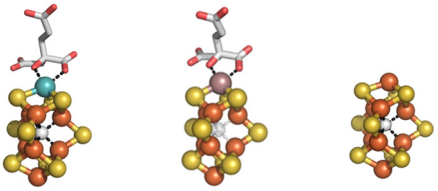

FIG 1 Structural models of M-cluster, V-cluster, and L-cluster. PYMOL was used to generate this figure. Atoms are colored as follows: Fe, orange; S, yellow; C, white; O, red; Mo, blue green; V, dark purple. The interstitial carbide is rendered transparent in the V-cluster to indicate that the presence of carbide in this cluster is yet to be demonstrated.

Consistent with the striking structural homology between the L-cluster and the two cofactors, the three clusters display similar catalytic capabilities in the solvent (*N*-methylformamide [NMF])-extracted state (16). All three clusters can catalyze the catalytic

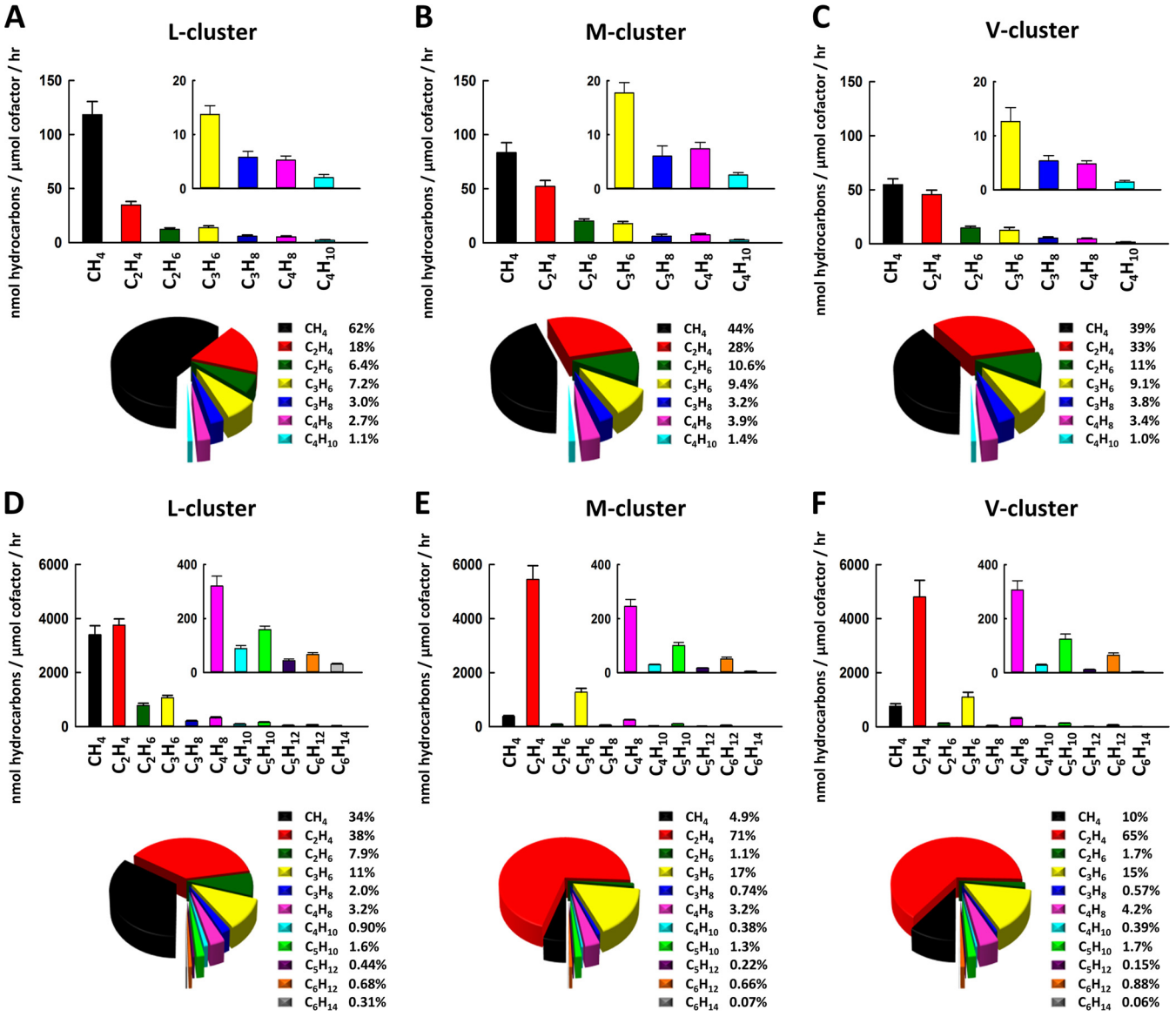

FIG 2 Formation of hydrocarbons from CO (A to C) and CN^- (D to F) reduction by L-cluster (A and D), M-cluster (B and E), and V-cluster (C and F). The specific activities are shown in the bar graphs, and the percent activities are shown in the pie charts in each panel. The specific activities of ammonia formation from CN^- were 23,494, 18,312, and 17,219 nmol NH_3/μmol cluster/h for L-cluster, M-cluster, and V-cluster, respectively.

reduction of CN^-, CO, and CO_2 to hydrocarbons (alkanes and alkenes; up to C_4 in length) in an ATP-independent, solvent-based assay, where samarium(II) iodide (SmI_2) and 2,6-lutidinium triflate (Lut-H) are used as a reductant (E_0'= −1.55 V in tetrahydrofuran [THF]) and a proton source, respectively (16). When a weaker reductant, europium(II) diethylenetriaminepentaacetate [Eu(II)-DTPA] (E_0'= −1.14 V at pH 8) is used in place of SmI_2 in an ATP-independent, buffer-based assay, no hydrocarbon products can be detected in the reactions of CO_2 reduction by the M- and V-clusters, and the turnover numbers (TON) of CO reduction by the two cofactors are reduced to 1/10. However, the efficiencies of both cofactors in the reaction of CN^- reduction remain largely unaffected, and perhaps more interestingly, both cofactors are capable of reducing CO and CN^- to longer hydrocarbons (alkanes and alkenes; up to C_7 in length) (17). This observation prompts the question of whether the L-cluster—an all-iron homolog of the two cofactors—displays the same catalytic behavior in the Eu(II)-DTPA-driven reactions of CO and CN^- reduction.

RESULTS AND DISCUSSION

Indeed, like the M- and V-clusters (17), the NMF-extracted L-cluster can reduce CO and CN^- to hydrocarbons in the same ATP-free buffer system under ambient conditions. The L-cluster forms methane (CH_4), ethene (C_2H_4), ethane (C_2H_6), propene (C_3H_6), propane (C_3H_8), 1-butene (C_4H_8), and *n*-butane (C_4H_{10}) as products of CO reduction (Fig. 2A). The L-cluster generates methane (CH_4), ethene (C_2H_4), ethane (C_2H_6), propene (C_3H_6), propane (C_3H_8), 1-butene (C_4H_8), *n*-butane (C_4H_{10}), 1-pentene (C_5H_{10}), *n*-pentane (C_5H_{12}), 1-hexene (C_6H_{12}), *n*-hexane

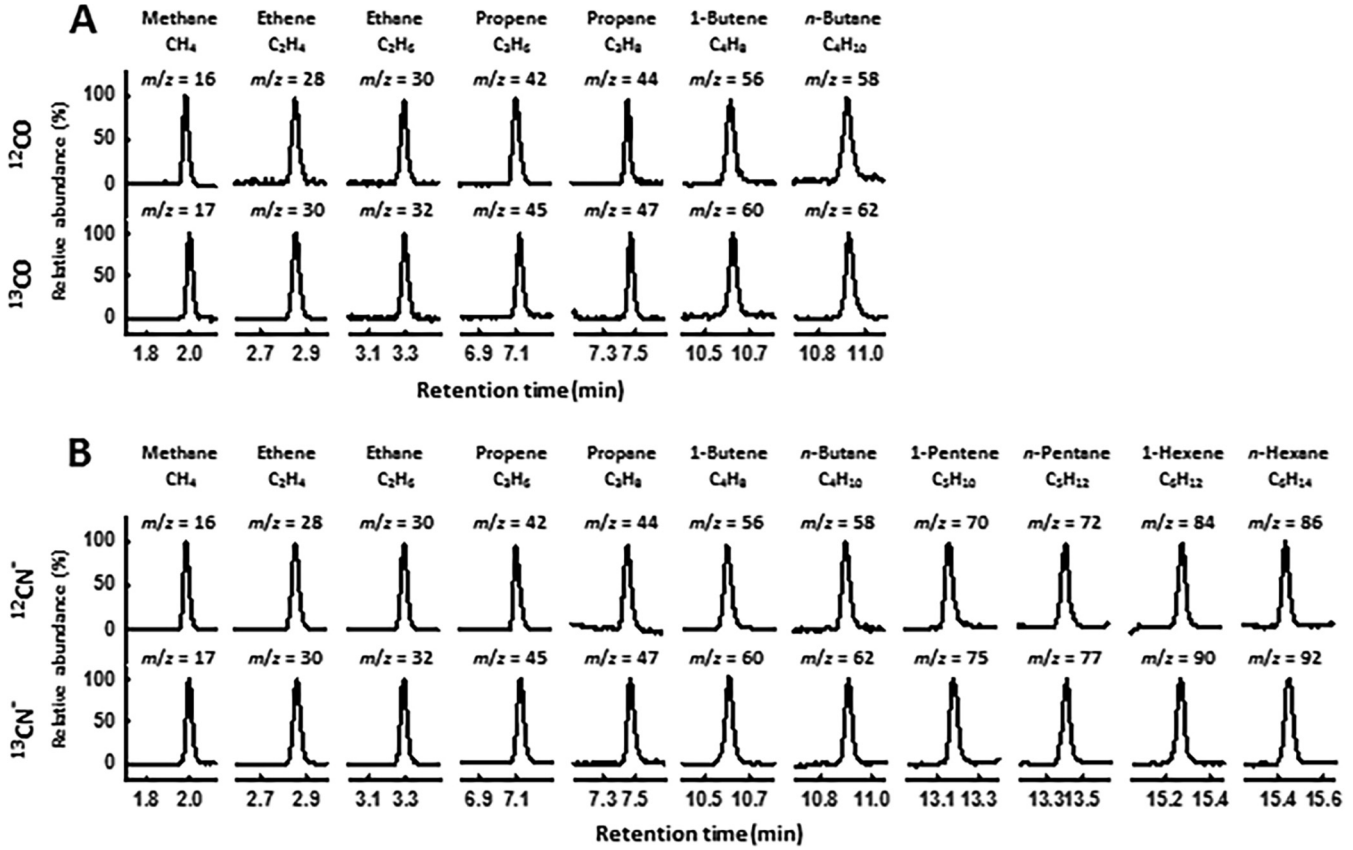

FIG 3 GC-MS analysis of hydrocarbons generated from the reduction of CO (A) and CN^- (B). Products were generated from the ^{12}C- or ^{13}C-labeled CO (A) and CN^- (B). The mass-to-charge (*m/z*) ratios at which the products were traced are indicated in the figure.

(C_6H_{14}), and ammonia (NH_3) as products of CN^- reduction (Fig. 2D). Gas chromatography-mass spectrometry (GC-MS) analysis further confirms CO and CN^- as the carbon sources for the hydrocarbons generated in these reactions, showing the mass shifts expected for all hydrocarbon products when ^{12}CO and $^{12}CN^-$ are replaced by ^{13}CO (Fig. 3A) and $^{13}CN^-$ (Fig. 3B), respectively. Compared to the M-cluster (Fig. 2B and E) and V-cluster (Fig. 2C and F), the L-cluster shows the same tendency to form longer hydrocarbons from CO and CN^- reduction in reactions driven by Eu(II)-DTPA (up to C_6) than hydrocarbons formed in reactions driven by SmI_2 (up to C_4), and it displays the same preference for CN^- over CO as a substrate for hydrocarbon formation (i.e., it reduces CN^- to longer hydrocarbons and at higher rates than CO [18]). Together, these observations not only highlight the structural-functional similarities of these cluster species but also suggest a nonessential impact of heterometal and/or homocitrate on their abilities to reduce CO and CN^- to hydrocarbons.

On the other hand, the all-iron L-cluster does differ from its Mo/homocitrate- and V/homocitrate-containing homologs in product distribution and deuterium effect. Compared to the M-cluster and V-cluster, the L-cluster generates a considerably larger portion of CH_4 from the reduction of CO (Fig. 2A versus B and C, black) and CN^- (Fig. 2D versus E and F, black), and it catalyzes the formation of products at a significantly higher alkane/alkene ratio, particularly in the presence of D_2O (Fig. 4A and C). Additionally, the ratio between product formation in D_2O and H_2O (F_D/F_H) increases almost linearly with the increasing length of the product in the reactions catalyzed by the M-cluster and V-cluster (Fig. 4B and D, circles and squares) but plateaus in the reactions catalyzed by the L-cluster (Fig. 4B and D, triangles). These observations point to a role of heterometal and/or homocitrate in modulating the CO and CN^- reactivity of the cluster.

The disparate CH_4 formation by the three clusters from CO and CN^- reduction can be further examined by the Anderson-Schulz-Flory (ASF) plots (19–21). The ASF plots are often used to predict the distribution of hydrocarbon products in the Fischer-Tropsch (FT) synthesis, an industrial process that parallels the reactions catalyzed by the nitrogenase cofactors in reducing CO to hydrocarbons (3, 4). These plots reveal a linear correlation between the probability of chain growth and the number of carbons for $\geq C_2$ products in the reactions of CO (Fig. 5A to C, black circles) and CN^- (Fig. 5D to F, black circles) reduction by all three clusters. However, except for the reduction of CO by the L-cluster (Fig. 5A, red circle), formation of the C_1 product (CH_4) in all other reactions deviates from the linear plot (Fig. 5B to F, red circles), suggesting a difference between the formation of the C_1 product and that of the $\geq C_2$ products in reaction site and/or pathway.

Overall, the data representing the formation of CH_4 fall below the linear ASF plots (Fig. 5, red circles), indicating that the amounts of CH_4 generated in these reactions are less than those predicted by the ASF equation. However, the fact that all three clusters generate larger quantities of CH_4 from CO than from CN^- (Fig. 2) is reflected by a notably lower degree of deviation of

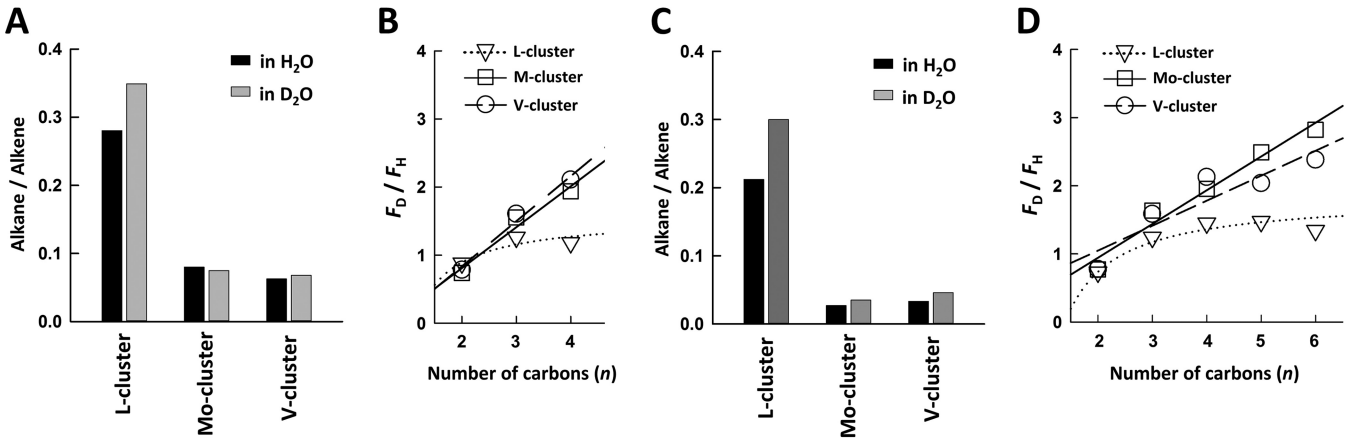

FIG 4 Ratios between alkanes (excluding CH_4) and alkenes generated from CO (A) and CN^- (C) reduction in the presence of H_2O and D_2O and ratios between products generated in D_2O and H_2O (F_D/F_H) from CO (B) and CN^- (D) reduction versus the number of carbons in the product. All ratios were calculated based on the percentage activities shown in the pie charts in Fig. 2.

CH_4 formation from the linear ASF plots (Fig. 5A versus D, B versus E, and C versus F, red circles). Furthermore, compared to M- and V-clusters, the L-cluster displays no deviation (Fig. 5A versus B and C, red circles) or little deviation (Fig. 5D versus E and F, red circles) of CH_4 formation from the linear ASF plots, which is consistent with the formation of a higher percentage of CH_4 by the L-cluster from the reduction of both CO and CN^- (Fig. 2).

One plausible explanation for the elevated level of CH_4 formation by the L-cluster is that this cluster contains a "free" Fe atom as an additional site for methanation in place of the heterometal sites that are covered up by homocitrate in the two cofactors. This theory would be consistent with the previously hypothesized heterogeneity of active sites in FT synthesis, which results in the deviation of product formation from ASF plots (22). Interestingly, an increase in reaction rate seems to be always accompanied by an increase in CH_4 formation and a concomitant decrease in the amount of longer hydrocarbons and/or the lengths of the hydrocarbon products formed by the three clusters. Such a trend can be observed when the "faster" SmI_2-driven reaction is compared with the "slower" Eu(II)-DTPA-driven reaction catalyzed by the same cluster (Fig. 6). This observation could reflect a competition between CH_4 formation/release and C−C coupling/chain extension, with the former favored by fast e^-/H^+ delivery and the latter facilitated by the opposite.

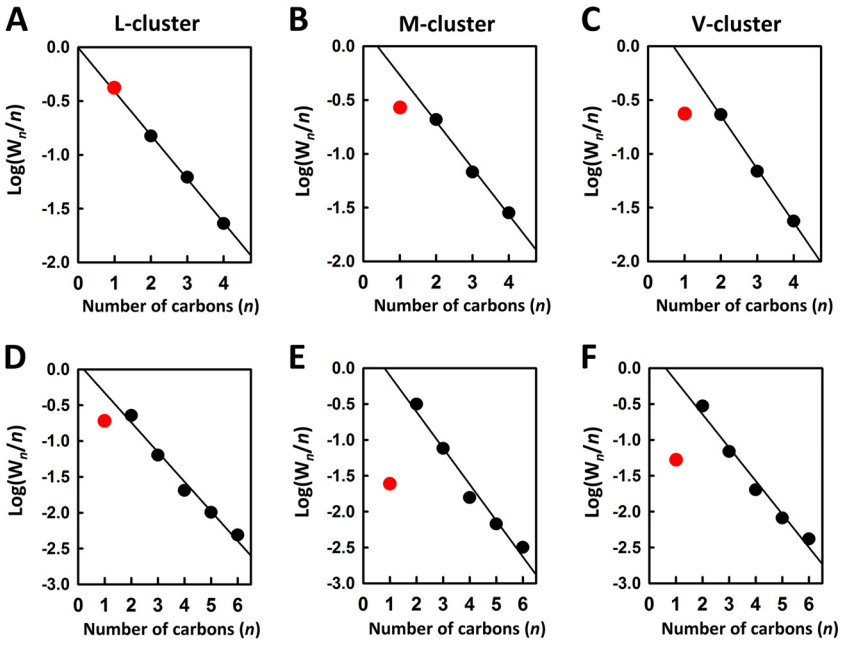

FIG 5 The Anderson-Schulz-Flory (ASF) plots of hydrocarbon formation from CO (A to C) and CN^- (D to F) reduction by L-cluster (A and D), M-cluster (B and E), and V-cluster (C and F). The plots were generated based on the logarithmic treatment of the ASF equation: $W_n = n\alpha^n(\ln_2\alpha)$, where W_n is the weight fraction of each product, n is the number of carbons in the product, and α is a constant that is referred to as the chain growth probability. This equation is used to describe the product distribution of the Fischer-Tropsch (FT) synthesis, the industrial process that combines CO and H_2 into hydrocarbons. The linear regression lines were generated by omitting the data of the C_1 product (i.e., CH_4), which is highlighted separately in red in each plot.

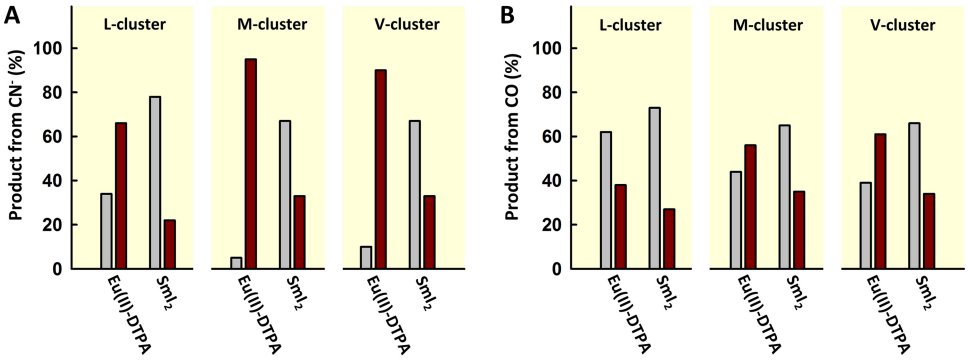

FIG 6 Product distributions of CN^- (A) and CO (B) reduction driven by Eu(II)-DPTA and SmI_2, respectively. Gray bars represent the percentages of CH_4 formation, whereas dark red bars represent the percentages of $\geq C_2$ hydrocarbon product formation in these reactions. The SmI_2-driven reaction data are from reference 14.

While the details of the multiple events that occur during the processes of CO and CN^- reduction require further investigation, the observation of differential CH_4 formation by the three clusters provides new insights into the mechanistic differences between these cofactor variants in catalyzing the reduction of carbonaceous compounds to hydrocarbons. The ability of the homocitrate-free, all-iron L-cluster to catalyze ATP/protein-independent hydrocarbon formation suggests the possibility of designing simpler synthetic clusters for industrial hydrocarbon production in the future. Additionally, it provides a unique platform for the investigation of the kinetic effects of deuterium without the interference of the protein environment and the heterometal/homocitrate components of the cluster. Systematic studies need to be conducted to understand these multifaceted kinetic effects, which may lead to significant insights into the mechanism of hydrocarbon formation by nitrogenase cofactors and homologs.

MATERIALS AND METHODS

Chemicals. Unless otherwise specified, all chemicals were purchased from Sigma-Aldrich (St. Louis, MO). Natural abundance ^{12}CO (99.5% purity) was purchased from Airgas (Lakewood, CA). All isotope-labeled compounds (≥98% isotopic purity) were purchased from Cambridge Isotopes (Andover, MA).

Protein purification and cofactor extraction. *Azotobacter vinelandii* strains expressing His-tagged NifEN, MoFe protein, and VFe protein were grown as described elsewhere (5, 11). Published methods were used for the purification of these nitrogenase proteins (5, 11). The L-, M-, and V-clusters were extracted into *N*-methylformamide (NMF) from 1.0 g NifEN, MoFe protein, and VFe protein, respectively, using a previously described method (6, 13).

CN^- and CO reduction by isolated clusters. A europium(II) diethylenetriamine pentaacetate [Eu(II)-DPTA] stock solution was prepared by dissolving equal molar amounts of europium(II) chloride and diethylenetriaminepentaacetic acid at a final concentration of 200 mM in 1 M Tris (pH 8.0) buffer. The reaction of CN^- reduction contained, in a total volume of 25 ml, 25 mM Tris (pH 7.8), 5 mM Eu(II)-DTPA (23), 0.45 μmol of isolate L-, M-, or V-cluster, and 100 mM NaCN. The reaction of CO reduction was of the same composition, except that 100% CO was used instead of NaCN. Both reactions were run at ambient temperature and pressure for different lengths of time. For gas chromatography (GC)-mass spectrometry (MS) experiments with isotope labels, natural abundance $Na^{12}CN$ and ^{12}CO were replaced by $Na^{13}CN$ and ^{13}CO, respectively.

Activity analysis of CN^- and CO reduction. Formation of products CH_4, C_2H_4, C_2H_6, C_3H_6, C_3H_8, 1-C_4H_8, *n*-C_4H_{10}, 1-C_5H_{10}, *n*-C_5H_{12}, 1-C_6H_{12}, *n*-C_6H_{14}, and *n*-C_7H_{16} was determined by gas chromatography on an activated alumina column (Grace, Deerfield, IL), which was held at 40°C for 2 min, heated to 200°C at 10°C/min, and held at 200°C for another 2 min. The 11 hydrocarbon products were quantified as described previously (3, 4), and their detection thresholds (in nanomoles per micromole of cofactor) were 1.1 (CH_4), 1.3 (C_2H_4), 1.3 (C_2H_6), 1.5 (C_3H_6), 1.3 (C_3H_8), 1.4 (1-C_4H_8), 1.4 (*n*-C_4H_{10}), 3.1 (1-C_5H_{10}), 3.7 (*n*-C_5H_{12}), 6.1 (1-C_6H_{12}), and 5.8 (*n*-C_6H_{14}).

Determination of cluster stability. The stability of the isolated L-cluster was determined by its ability to reconstitute the apo form of the NifEN protein after incubation with the buffer system used for Eu(II)-DPTA-driven reactions of CO and CN^- reduction (Fig. 7). Specifically, the isolated L-cluster was incubated with the buffer system for various lengths of time before addition of the apo form of NifEN to the mixture, resulting in an L-cluster-reconstituted, holo form of NifEN. Subsequently, the holo form of NifEN was incubated with MgATP, dithionite, MoO_4^{2-}, homocitrate, NifH, and apo form of MoFe protein, during which process the L-cluster was matured to an M-cluster on NifEN and transferred to the apo form of the MoFe protein, resulting in an M-cluster reconstituted, holo form of MoFe protein that could then be assayed for activity (24).

GC-MS. The hydrocarbon products were identified by GC-MS using Hewlett-Packard 5890 GC and 5972 mass selective detector (MSD). The identities of CH_4, C_2H_4, C_2H_6, C_3H_6, C_3H_8, 1-C_4H_8, *n*-C_4H_{10}, 1-C_5H_{10}, *n*-C_5H_{12}, 1-C_6H_{12}, and *n*-C_6H_{14} were confirmed by comparing their

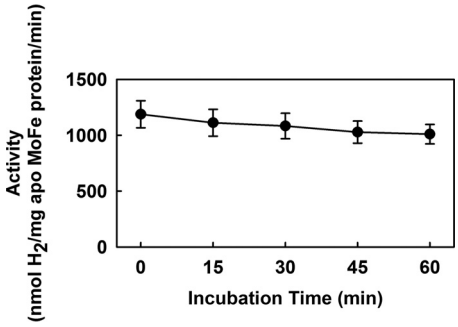

FIG 7 Stability of the isolated L-cluster in the ATP-free buffer system used in this study. After incubation with this buffer for various lengths of time, the integrity of the L-cluster was determined by its ability to reconstitute the L-cluster-deficient apo form of the NifEN protein. Data are presented as means ± standard deviations (SD) (error bars) ($n = 5$).

masses and retention times with those of the Scott standard *n*-alkane and 1-alkene gas mixture (Scott Specialty Gases, Inc., Plumsteadville, PA). A total of 50 μl gas was injected into a split/splitless injector operated at 125°C in splitless mode. A 1-mm-inner-diameter (i.d.) liner was used to optimize sensitivity. Gas separation was achieved on a Restek (Bellafonte, PA) PLOT-QS capillary column (0.320 mm [i.d.] by 30 m [length]), which was held at 40°C for 1 min, heated to 220°C at 10°C/min, and held at 220°C for another 3 min. The carrier gas, helium, was passed through the column at 1.0 ml/min. The mass spectrometer was operated in electron impact (EI) ionization and selected ion monitoring (SIM) mode.

ACKNOWLEDGMENTS

We thank Douglas Rees and Nathan Dalleska of Caltech (Pasadena) for help with GC-MS analysis.

This work was supported by NIH grant GM-67626 (M.W.R.).

REFERENCES

1. **Burgess BK, Lowe DJ**. 1996. Mechanism of molybdenum nitrogenase. Chem Rev **96:**2983–3012. http://dx.doi.org/10.1021/cr950055x.
2. **Eady RR**. 1996. Structure-function relationships of alternative nitrogenases. Chem Rev **96:**3013–3030. http://dx.doi.org/10.1021/cr950057h.
3. **Lee CC, Hu Y, Ribbe MW**. 2010. Vanadium nitrogenase reduces CO. Science **329:**642. http://dx.doi.org/10.1126/science.1191455.
4. **Hu Y, Lee CC, Ribbe MW**. 2011. Extending the carbon chain: hydrocarbon formation catalyzed by vanadium/molybdenum nitrogenases. Science **333:**753–755. http://dx.doi.org/10.1126/science.1206883.
5. **Lee CC, Hu Y, Ribbe MW**. 2009. Unique features of the nitrogenase VFe protein from *Azotobacter vinelandii*. Proc Natl Acad Sci U S A **106:**9209–9214. http://dx.doi.org/10.1073/pnas.0904408106.
6. **Fay AW, Blank MA, Lee CC, Hu Y, Hodgson KO, Hedman B, Ribbe MW**. 2010. Characterization of isolated nitrogenase FeVco. J Am Chem Soc **132:**12612–12618. http://dx.doi.org/10.1021/ja1019657.
7. **Schindelin H, Kisker C, Schlessman JL, Howard JB, Rees DC**. 1997. Structure of ADPxAIF$_4^-$ stabilized nitrogenase complex and its implications for signal transduction. Nature **387:**370–376. http://dx.doi.org/10.1038/387370a0.
8. **Kim J, Rees DC**. 1992. Structural models for the metal centers in the nitrogenase molybdenum-iron protein. Science **257:**1677–1682. http://dx.doi.org/10.1126/science.1529354.
9. **Einsle O, Tezcan FA, Andrade SL, Schmid B, Yoshida M, Howard JB, Rees DC**. 2002. Nitrogenase MoFe-protein at 1.16-A resolution: a central ligand in the FeMo-cofactor. Science **297:**1696–1700. http://dx.doi.org/10.1126/science.1073877.
10. **Lancaster KM, Roemelt M, Ettenhuber P, Hu Y, Ribbe MW, Neese F, Bergmann U, DeBeer S**. 2011. X-ray emission spectroscopy evidences a central carbon in the nitrogenase iron-molybdenum cofactor. Science **334:**974–977. http://dx.doi.org/10.1126/science.1206445.
11. **Hu Y, Fay AW, Ribbe MW**. 2005. Identification of a nitrogenase FeMo cofactor precursor on NifEN complex. Proc Natl Acad Sci U S A **102:**3236–3241. http://dx.doi.org/10.1073/pnas.0409201102.
12. **Corbett MC, Hu Y, Fay AW, Ribbe MW, Hedman B, Hodgson KO**. 2006. Structural insights into a protein-bound iron-molybdenum cofactor precursor. Proc Natl Acad Sci U S A **103:**1238–1243. http://dx.doi.org/10.1073/pnas.0507853103.
13. **Fay AW, Blank MA, Lee CC, Hu Y, Hodgson KO, Hedman B, Ribbe MW**. 2011. Spectroscopic characterization of the isolated iron-molybdenum cofactor (FeMoco) precursor from the protein NifEN. Angew Chem Int Ed Engl **50:**7787–7790. http://dx.doi.org/10.1002/anie.201102724.
14. **Lancaster KM, Hu Y, Bergmann U, Ribbe MW, DeBeer S**. 2013. X-ray spectroscopic observation of an interstitial carbide in NifEN-bound FeMoco precursor. J Am Chem Soc **135:**610–612. http://dx.doi.org/10.1021/ja309254g.
15. **Wiig JA, Hu Y, Lee CC, Ribbe MW**. 2012. Radical SAM-dependent carbon insertion into the nitrogenase M-cluster. Science **337:**1672–1675. http://dx.doi.org/10.1126/science.1224603.
16. **Lee CC, Hu Y, Ribbe MW**. 2015. Catalytic reduction of CN^-, CO, and CO_2 by nitrogenase cofactors in lanthanide-driven reactions. Angew Chem Int Ed Engl **54:**1219–1222. http://dx.doi.org/10.1002/anie.201410412.
17. **Lee CC, Hu Y, Ribbe MW**. 2012. ATP-independent formation of hydrocarbons catalyzed by isolated nitrogenase cofactors. Angew Chem Int Ed Engl **51:**1947–1949. http://dx.doi.org/10.1002/anie.201108916.
18. **Pickett CJ, Vincent KA, Ibrahim SK, Gormal CA, Smith BE, Fairhurst SA, Best SP**. 2004. Synergic binding of carbon monoxide and cyanide to the FeMo cofactor of nitrogenase: relic chemistry of an ancient enzyme? Chemistry **10:**4770–4776. http://dx.doi.org/10.1002/chem.200400382.
19. **Schulz GV**. 1936. The dispersal of molecular weight in high polymer mixtures and the determination of median molecular weights. 134 announcement on high polymer bonding. Z Physiol Chem **32:**27–45.
20. **Flory PJ**. 1936. Molecular size distribution in linear condensation polymers. J Am Chem Soc **58:**1877–1885. http://dx.doi.org/10.1021/ja01301a016.
21. **Friedel RA, Anderson RB**. 1950. Composition of synthetic liquid fuels. I. Product distribution and analysis of C_5-C_8 paraffin isomers from cobalt catalyst. J Am Chem Soc **72:**2307. http://dx.doi.org/10.1021/ja01161a536.
22. **Puskas I, Hurlbut RS**. 2003. Comments about the causes of deviations from the Anderson-Schulz-Flory distribution of the Fischer-Tropsch reaction products. Catal Today **84:**99–109. http://dx.doi.org/10.1016/S0920-5861(03)00305-5.
23. **Vincent KA, Tilley GJ, Quammie NC, Streeter I, Burgess BK, Cheesman MR, Armstrong FA**. 2003. Instantaneous, stoichiometric generation of powerfully reducing states of protein active sites using Eu(II) and polyaminocarboxylate ligands. Chem Commun **20:**2590–2591. http://dx.doi.org/10.1039/b308188e.
24. **Fay AW, Lee CC, Wiig JA, Hu Y, Ribbe MW**. 2011. Protocols for cofactor isolation of nitrogenase. Methods Mol Biol **766:**239–248. http://dx.doi.org/10.1007/978-1-61779-194-9_16.